Effective Weld Properties for Hollow Structural Section T-Connections under Branch In-Plane Bending

MATTHEW R. MCFADDEN and JEFFREY A. PACKER

Abstract

The 2010 AISC *Specification for Structural Steel Buildings* has expanded the scope in Chapter K, "Design of HSS and Box Member Connections," to include a Section K4, "Welds of Plates and Branches to Rectangular HSS." An experimental program was undertaken to test various unreinforced HSS-to-HSS 90° T-connections subject to branch in-plane bending moment with the objective of determining the effectiveness of the welded joint. Twelve unique test specimens were designed to be weld-critical, and the results from the full-scale tests revealed that the current equation for the effective elastic section modulus for in-plane bending, S_{ip}, given in Table K4.1 of AISC 360-10, is very conservative. A modification to the current requirement that limits the effective width of the transverse weld elements is proposed, resulting in a safe but more economical weld design method for HSS-to-HSS T-connections subject to branch bending moment. By reanalyzing the data of prior weld-critical tests on HSS-to-HSS T- and X- (cross-) connections subject to branch axial loading, it is shown that the proposed new weld effective length recommendation is applicable to these connections as well. It is also concluded that the fillet weld directional strength enhancement factor, $(1.00 + 0.50\sin^{1.5}\theta)$, should not be used for strength calculations of welded joints to square and rectangular HSS, with the proposed revision, when the effective length method is used.

Keywords: hollow structural sections, welded joints, moment connections, gas-metal arc welding, effective weld properties, fillet welds, partial-joint-penetration flare-bevel-groove welds.

INTRODUCTION

The design criteria for fillet welds have evolved over the years as more data have become available through experimental research. While often viewed as simplistic in nature, the way in which a fillet weld transfers the load through a connection can be complex, especially in semi-rigid connections between rectangular and square hollow structural sections (HSS). Because welding can only be performed around the outer perimeter of HSS walls and because the majority of connections between HSS are fillet-welded, the fillet welds are inherently eccentrically loaded, which causes secondary bending moments at the root.

With welded connections between HSS there are currently two design methods used for weld design (Packer, Sherman and Lecce, 2010):

1. The welds may be proportioned to develop the yield strength of the connected branch wall at all locations around the branch perimeter. This method will produce an upper limit on the required weld size and may be excessively conservative in some situations.

Matthew R. McFadden, Project Engineer/Bridge Designer, MMM Group, Ottawa, ON, Canada. E-mail: matthew_mcfadden@outlook.com

Jeffrey A. Packer, Bahen/Tanenbaum Professor of Civil Engineering, University of Toronto, Toronto, ON, Canada (corresponding). E-mail: jeffrey.packer@utoronto.ca

2. The welds may be designed as "fit-for-purpose" and proportioned to resist the applied forces in the branch. The highly nonuniform distribution of stress around the weld perimeter due to the relative flexibility of the connecting HSS face requires the use of effective weld lengths. This approach may potentially result in smaller weld sizes, thus providing a more economical design with improved aesthetics.

The design methods for fillet welds to develop the yield strength of the connected branch wall at all locations around the perimeter in various national and international codes, specifications and guidelines are reviewed and compared in McFadden, Sun and Packer (2013). In that paper, the equations were rearranged to solve for the minimum required effective weld throat (t_w) per unit length of the weld in terms of the branch wall thickness (t_b) for the simple case of an axially loaded HSS-to-HSS T-connection ($\theta = 90°$), using the equivalent of cold-formed HSS made to ASTM A500 Grade C (ASTM, 2010) with matching electrodes. That exercise demonstrated a considerable disparity in fillet weld design criteria.

Modern design methods based on data from full-scale tests of weld-critical connections between HSS performed at the University of Toronto (Frater and Packer, 1992a, 1992b; Packer and Cassidy, 1995) have led to the development and use of effective weld properties. These properties take into account the nonuniform distribution of normal stress and strain around the weld perimeter and exclude portions of the weld that are ineffective in resisting the applied loads.

The latest (third edition) of the International Institute of Welding (IIW) recommendations (IIW, 2012) requires that the design resistance of hollow section connections be based on failure modes that do not include weld failure, with the latter being avoided by satisfying either of the following criteria:

1. Welds are to be proportioned to achieve the capacity of the connected member walls.
2. Welds are to be proportioned as "fit-for-purpose" and to resist forces in the connected members, taking account of connection deformation/rotation capacity and considering weld effective lengths.

This document (IIW, 2012) thus specifically acknowledges the effective length concept for designing welds between HSS. The preceding two options for weld design are also adopted in an informative Annex to ISO 14346 (2013).

American Codes and Specifications

Specific design criteria for HSS connections (statically and cyclically loaded) are given in Clause 2, Design of Welded Connections, Part D, of AWS D1.1 (2010) and used with the applicable requirements of Part A. Those provisions may be used in conjunction with governing steel design specifications, such as AISC 360 (2010), to determine the strength of structural steel members or connections.

In Section K4 of AISC 360 (2010), a detailed design method considering effective weld properties for predominantly statically loaded HSS-to-HSS connections is given. The available strength of such connections incorporates the nonuniform load transfer around the perimeter of the weld due to differences in the relative flexibilities of the chord loaded normal to its surface and membrane stresses carried by the branch parallel to its surface. The nominal strengths of connections subject to branch axial load or bending are based on the limit state of shear rupture along the plane of the effective weld throat and are calculated as follows:

$$R_n \text{ or } P_n = F_{nw} t_w l_e \qquad \text{Spec. Eq. (K4-1)} \quad (1)$$

$$M_{n-ip} = F_{nw} S_{ip} \qquad \text{Spec. Eq. (K4-2)} \quad (2)$$

$$M_{n-op} = F_{nw} S_{op} \qquad \text{Spec. Eq. (K4-3)} \quad (3)$$

where the LRFD resistance factor, ϕ, applied to the nominal strength values is equal to 0.75 and 0.80 for fillet welds and partial-joint-penetration (PJP) flare-bevel-groove welds, respectively.

The nominal stress of the weld metal, F_{nw}, for fillet welds and PJP groove welds, specified in Table J2.5 of AISC 360 (2010), is taken as 0.60 multiplied by the minimum tensile strength of the weld metal, F_{EXX}, for fillet welds subject to shear and PJP groove welds subject to tension normal to the weld axis. The use of a directional strength enhancement factor for fillet welds in HSS-to-HSS connections is currently not allowed when the effective length method is used (AISC, 2010; Packer et al., 2010).

The effective weld properties associated with Equations 1, 2 and 3 for T-, Y- and X- (cross-) connections (e.g., Figure 1a) under branch axial load or bending are specified in Table K4.1 of AISC 360 (2010) and summarized as follows:

Branch axial load:

$$l_e = \frac{2H_b}{\sin\theta} + 2b_{eoi} \qquad \text{Spec. Eq. (K4-5)} \quad (4)$$

Branch in-plane bending:

$$S_{ip} = \frac{t_w}{3}\left(\frac{H_b}{\sin\theta}\right)^2 + t_w b_{eoi}\left(\frac{H_b}{\sin\theta}\right) \qquad \text{Spec. Eq. (K4-6)} \quad (5)$$

Branch out-of-plane bending:

$$S_{op} = t_w\left(\frac{H_b}{\sin\theta}\right)B_b + \frac{t_w}{3}\left(B_b^2\right) - \frac{\left(t_w/3\right)\left(B_b - b_{eoi}\right)^3}{B_b} \qquad \text{Spec. Eq. (K4-7)} \quad (6)$$

where b_{eoi} is equal to:

$$b_{eoi} = \frac{10}{B/t}\left(\frac{F_y t}{F_{yb} t_b}\right)B_b \le B_b \qquad \text{Spec. Eq. (K2-13)} \quad (7)$$

Also, for connections with $\beta > 0.85$ or $\theta > 50°$, $b_{eoi}/2$ shall not exceed $2t$.

The weld effective length in Equation 4 was—for consistency—made equivalent to the branch wall effective lengths used in Section K2.3 of AISC 360 (2010) for the limit state of local yielding of the branch(es) due to uneven load distribution, which in turn is based on IIW (1989). The effective width of the individual weld element transverse to the chord, b_{eoi}, is illustrated in Figure 1b. This term was empirically derived on the basis of laboratory tests in the 1970s and 1980s (Davies and Packer, 1982). The effective elastic section modulus of welds for in-plane bending and out-of-plane bending, S_{ip} (Equation 5) and S_{op} (Equation 6), respectively, apply in the presence of the bending moments, M_{ip} and M_{op} (as shown in Figure 1). Equation 5 is derived from:

$$I_{ip} = 2 \times \frac{t_w}{12}\left(\frac{H_b}{\sin\theta}\right)^3 + 4t_w\left(\frac{b_{eoi}}{2}\right)\left(\frac{H_b}{2\sin\theta}\right)^2 \tag{8}$$

$$= \frac{t_w}{6}\left(\frac{H_b}{\sin\theta}\right)^3 + 4t_w\left(\frac{t_w b_{eoi}}{2}\right)\left(\frac{H_b}{\sin\theta}\right)^2$$

and substituted into:

$$S_{ip} = \frac{I_{ip}}{\left(H_b/2\sin\theta\right)} \tag{9}$$

In a similar manner, Equation 6 is derived from:

$$I_{op} = 2\times\left[t_w\left(\frac{H_b}{\sin\theta}\right)\left(\frac{B_b}{2}\right) + \frac{t_w}{12}\left(B_b^3\right) - \frac{t_w}{12}\left(B_b - b_{eoi}\right)^3\right]$$

$$= \frac{t_w}{2}\left(\frac{H_b}{\sin\theta}\right)\left(B_b^2\right) + \frac{t_w}{6}\left(B_b^3\right) - \frac{t_w}{6}\left(B_b - b_{eoi}\right)^3 \tag{10}$$

and substituted into:

$$S_{op} = \frac{I_{op}}{\left(B_b/2\right)} \tag{11}$$

While being based on informed knowledge of general HSS connection behavior, Equations 5 and 6 have not been substantiated by tests, and therefore are purely speculative.

EXPERIMENTAL PROGRAM

An experimental program was performed at the University of Toronto to test various unreinforced HSS-to-HSS 90° T-connections subject to branch in-plane bending. The objective of the study was to investigate the effectiveness of the weld in resisting the forces at the ultimate limit state of weld rupture and verify or adjust the current effective weld properties postulated in Section K4 of AISC 360 (2010) for such connections. Details of the design procedure, fabrication process, test setup assembly and instrumentation are discussed herein.

Design Procedure for Weld-Critical Connections

Twelve test specimens were designed to be weld-critical under the application of branch in-plane bending moments. Cold-formed HSS made to ASTM A500 Grade C (ASTM, 2010) were used for all branch and chord members in the experimental program. Their geometric configurations were selected based on available materials and key parameters that influence connection strength and behavior: branch-to-chord width ratio (β-ratio) and chord wall slenderness value. The outside dimensions of the chord remained constant (8 × 8 in.) for all test specimens to facilitate ease of setup and takedown in the testing rig. Nominal wall thicknesses of ¼, ⅜ and ½ inch were selected and correspond to chord wall slenderness values of 34, 23 and 17, respectively, when considering the design wall thickness (AISC, 2010). Outside dimensions of the branch members were 2 × 2, 4 × 4, 6 × 6 and 8 × 8 inches with β-ratios equal to 0.25, 0.50, 0.75 and 1.00, respectively. The combination of β-ratios and chord wall slenderness values gave a range of potential failure modes, including chord wall plastification, branch flexural failure and local yielding of the branches due to uneven load distribution. Experimental designation, chord and branch dimensions, key parameters, connection predicted failure modes and nominal LRFD connection flexural strengths for the individual test specimens are presented in Table 1.

Test specimens with $0.25 \le \beta \le 0.85$ are classified as

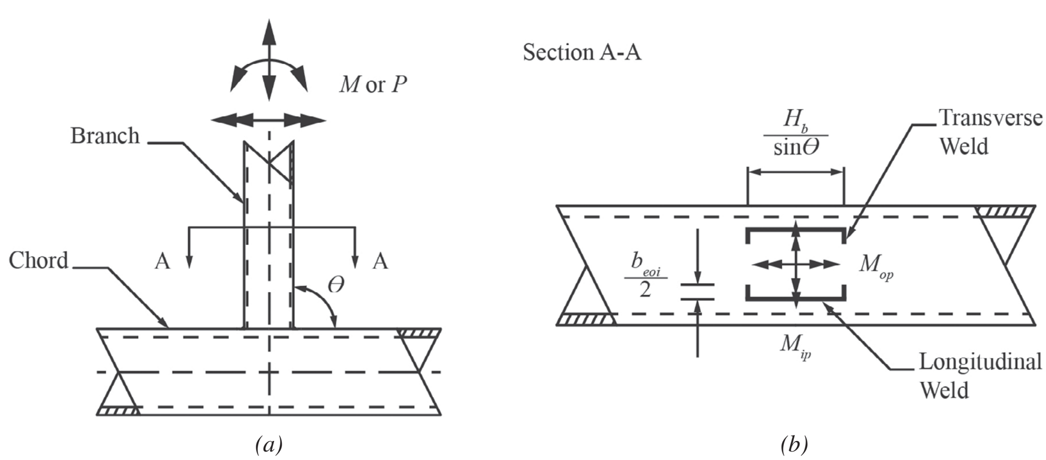

Fig. 1. Weld effective length terminology for T-, Y-, and X- (cross-) connections under branch axial load or bending: (a) various load cases; (b) weld effective length dimensions.

Experimental Designation	Chord Designation (in.)	Branch Designation (in.)	Chord Wall Slenderness Value	β-Ratio	Connection Failure Mode†	LRFD Flexural Strength ϕM_n (kip-ft)
T-0.25-34	HSS 8×8×¼	HSS 2×2×¼	34	0.25	CW	2.09
T-0.25-23	HSS 8×8×⅜	HSS 2×2×¼	23	0.25	BF	3.62
T-0.25-17	HSS 8×8×½	HSS 2×2×¼	17	0.25	BF	3.62
T-0.50-34	HSS 8×8×¼	HSS 4×4×¼	34	0.50	CW	4.35
T-0.50-23	HSS 8×8×⅜	HSS 4×4×¼	23	0.50	CW	9.79
T-0.50-17	HSS 8×8×½	HSS 4×4×½	17	0.50	CW	17.4
T-0.75-34	HSS 8×8×¼	HSS 6×6×¼	34	0.75	CW	10.4
T-0.75-23	HSS 8×8×⅜	HSS 6×6×⅜	23	0.75	CW	23.3
T-0.75-17	HSS 8×8×½	HSS 6×6×½	17	0.75	CW	41.4
T-1.00-34	HSS 8×8×¼	HSS 8×8×¼	34	1.00	BY	39.4
T-1.00-23	HSS 8×8×⅜	HSS 8×8×⅜	23	1.00	BY	66.5
T-1.00-17	HSS 8×8×½	HSS 8×8×½	17	1.00	BY	99.1

Table 1. Test Specimen Member Sizes, Key Parameters, Predicted Failure Modes and Connection Nominal Design Strengths

† CW—chord wall plastification; BF—branch flexural failure; BY—local yielding of branch due to uneven load distribution

stepped connections, while those with $0.85 < \beta \leq 1.00$ are classified as matched connections. Their general configurations are depicted in Figures 2a and 2b. Stepped connections have a continuous fillet weld around the branch footprint, whereas matched connections have a fillet weld along the branch transverse walls and a PJP groove weld along the branch longitudinal walls. A transitional zone between the two types of welds exists at the branch corners.

Welds were designed to ensure that weld rupture preceded connection failure, whereby the predicted nominal flexural strength of the weld ($M_{n\text{-}ip}$) was less than the predicted LRFD flexural strength of the test specimen (ϕM_n). Weld sizes were initially selected based on standard sizes specified in AWS D1.1 (2010) satisfying the minimum requirements in Tables J2.3 and J2.4 of AISC 360 (2010) for PJP groove welds and fillet welds, respectively. Matching electrodes with a nominal tensile strength of 70 ksi were used for the calculations.

Test Specimen Fabrication Process

The welded joints were executed by an industrial robot modified to perform gas-metal arc welding (GMAW) at the Automation Division of Lincoln Electric's headquarters in Cleveland, Ohio. The welding equipment used throughout fabrication included a Fanuc ARC Mate 120iC 10L robotic arm, Fanuc system R-30iA power supply, Lincoln Electric PowerWave 455M/STT and 655 robotic welders, and an automatic wire feeder.

A 0.035-in.-diameter AWS ER70S-6 (SuperGlide S6) solid wire electrode with a nominal specified tensile strength of 70 ksi and a shielding gas mixture of 90% argon and 10% carbon dioxide supplied at a rate of 40 cubic feet per hour (CFH) was used to weld the test specimens. Welding process parameters recommended by the Lincoln Electric 2010 Welding Consumables Product Catalogue were used as a starting point, and adjusted throughout the fabrication

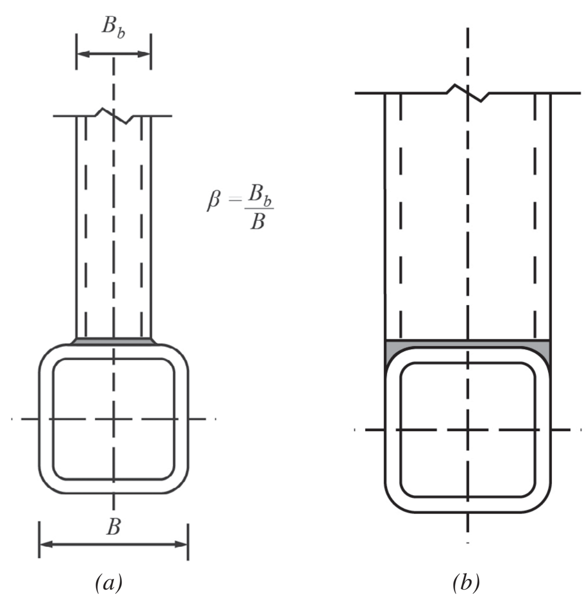

Fig. 2. HSS-to-HSS T-connection classification:
(a) side elevation of a stepped connection ($0.25 \leq \beta \leq 0.85$);
(b) side elevation of a matched connection ($0.85 < \beta \leq 1.00$).

process as necessary. To satisfy the qualification requirements of AWS D1.1 (2010) for prequalified welded joints, numerous trial specimens were created and macroetched before welding the actual test specimens. The macroetch specimens were used to calibrate the welding process parameters to achieve the desired weld size, profile, fusion with the base metal and root penetration for each joint.

Stepped connections were clamped to a level table and welded in the horizontal position. Matched connections were mounted to rotating chucks and welded in the flat position using coordinated motion. Root pass welds along the corner radii of the chord adjacent to the longitudinal PJP groove weld elements were required for the matched connections.

Once completed, the welded joints were inspected in accordance with the visual inspection acceptance criteria in Clause 6 of AWS D1.1 (2010). Discontinuities such as crack prohibition, undercut, porosity, weld profile and weld size were investigated. No discontinuities exceeding the allowable limits of the visual inspection acceptance criteria were observed.

Test Setup and Instrumentation

The test setup assembly is shown in Figure 3, wherein the vertical HSS branch is pulled laterally by the actuator (1) to create a bending moment in the branch and thus the connection and HSS chord. The testing arrangement was designed to minimize out-of-plane effects applied to the test specimen, to allow the branch member to deflect both horizontally and vertically without inducing restraint forces and to simply support the chord ends.

Unidirectional strain gages oriented along the longitudinal axis of the branch were installed at numerous locations around the branch perimeter to measure the nonuniform distribution of normal strain around its footprint, as well as to monitor out-of-plane effects during testing. The strain gages were placed approximately $\frac{9}{16}$ in. above the vertical fillet weld toe to avoid the high strain region immediately adjacent to the toe caused by notch effects. Additional strain gages were placed at all four branch mid-wall locations in the constant stress region, which is located at least three times the branch width ($3B_b$) away from the connection

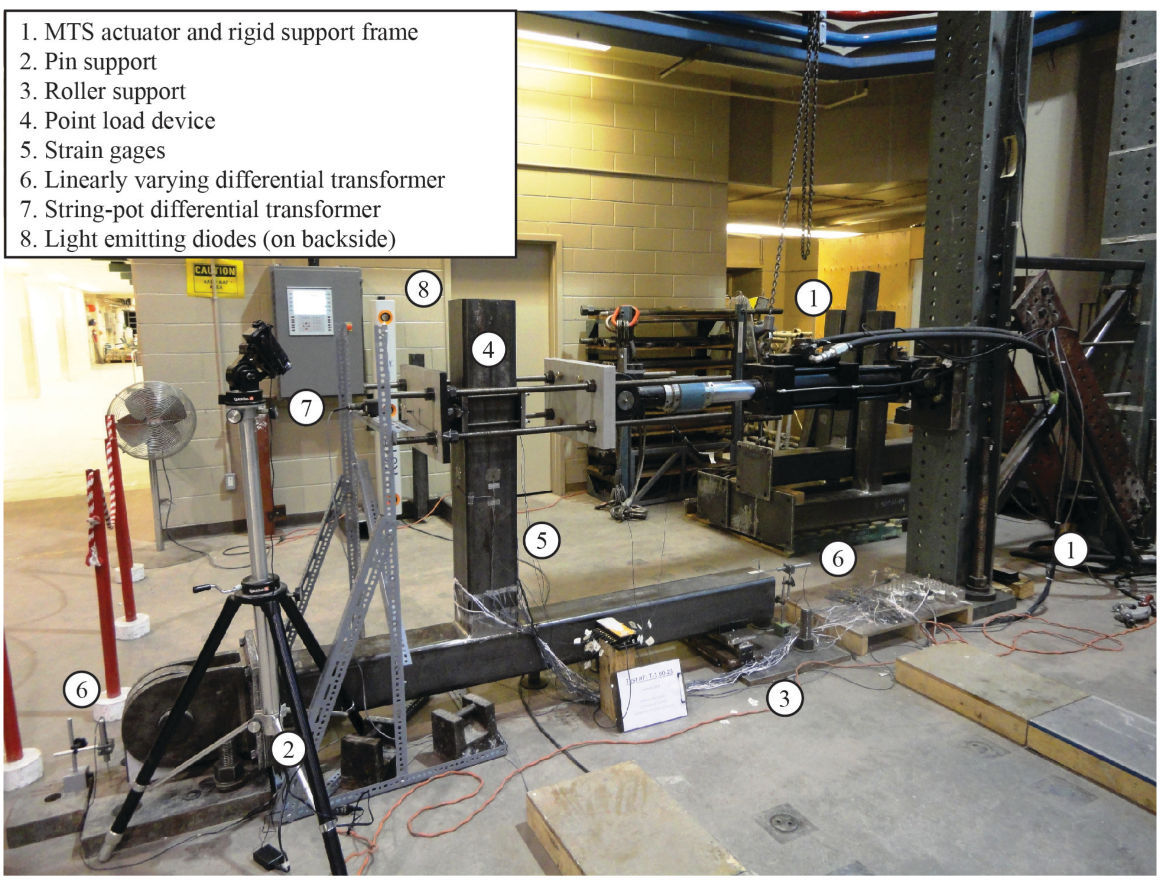

Fig. 3. Elevation of the general test setup assembly for full-scale experiments.

Table 2. Average Measured Cross-Sectional Dimensions of HSS					
HSS Designation (in.)	**Height and Width, *H* and *B* (in.)**	**Wall Thickness, *t* (in.)**	**Cross-Sectional Area, *A* (in.^{2})**	**Outer Corner Radius (in.)**	**Inner Corner Radius (in.)**
HSS 2×2×¼	2.01	0.227	1.52	0.482	0.248
HSS 4×4×¼	4.02	0.225	3.34	0.492	0.282
HSS 4×4×½	4.02	0.458	6.11	0.945	0.476
HSS 6×6×¼	6.01	0.226	5.13	0.509	0.298
HSS 6×6×⅜	6.00	0.342	7.48	0.772	0.416
HSS 6×6×½	6.01	0.459	9.67	1.16	0.671
HSS 8×8×¼	8.02	0.232	7.06	0.639	0.398
HSS 8×8×⅜	7.99	0.344	10.1	0.939	0.588
HSS 8×8×½	8.05	0.456	13.1	1.36	0.875

Table 3. HSS Tensile Coupon Test Results						
HSS Designation (in.)	**F_y* (ksi)**	**ε_y ($\times 10^3$ $\mu\varepsilon$)**	**F_u (ksi)**	**ε_u (%)**	**E ($\times 10^3$ ksi)**	**F_y/F_u**
HSS 2×2×¼	59.3	2.27	67.5	21.3	26.2	0.879
HSS 4×4×¼	62.1	1.99	76.2	27.3	31.1	0.815
HSS 4×4×½	63.9	2.58	79.1	26.4	24.8	0.808
HSS 6×6×¼	48.0	1.86	63.6	33.2	25.8	0.755
HSS 6×6×⅜	50.7	1.94	61.5	33.9	26.2	0.824
HSS 6×6×½	53.8	2.03	64.3	34.0	26.5	0.837
HSS 8×8×¼	55.4	2.07	71.5	27.5	26.9	0.775
HSS 8×8×⅜	57.1	2.24	73.9	32.3	25.5	0.773
HSS 8×8×½	59.8	2.24	73.8	34.2	26.8	0.810

* Determined by the 0.2% strain offset method.

(Mehrotra and Govil, 1972). These were used to monitor out-of-plane effects during testing, which were observed to be insignificant.

To determine the branch deflection profile and chord wall deformation profiles throughout testing, a K610 optical camera was used to record the coordinates of strobing light-emitting diodes (LEDs). The LEDs were mounted to the test specimens and test setup assembly in various locations to record their x, y and z coordinates. The force components applied to the branch were used to calculate the in-plane moment, out-of-plane moment and torsion acting on the connection.

EXPERIMENTAL RESULTS

Geometric and Material Properties of HSS

All HSS cross-sectional dimensions were measured at multiple points. Cross-sections of each HSS used in the experimental program were saw-cut at least 12 in. away from the flame-cut ends of the parent tube and then machined normal to the longitudinal axis. They were scanned and traced using software with built-in measuring tools to determine the cross-sectional area, outside dimensions and outer/inner corner radii. Wall thicknesses were measured using a 1.0-in. Mitutoyo Digimatic Micrometer (accurate to ±0.00005 in.). The average geometric properties are given in Table 2.

The results from 27 individual tensile coupon (TC) tests are summarized in Table 3. Three TCs for each HSS used in the experimental program were tested in accordance with the standard methods for tension testing of metallic materials (ASTM, 2008). As required by ASTM A500 (ASTM, 2010), these TCs were saw-cut from the flat faces of the HSS not containing the seam weld and in the longitudinal direction. For each of the nine HSS sizes (Table 2), one TC was taken at the mid-width of the three HSS walls not containing the seam weld. The ductility of the material was generally well beyond the minimum specified requirement (21% elongation).

Geometric and Material Properties of As-Laid Welds

The actual effective throat thickness of fillet-welded joints tested in the experimental program was measured after testing. Several macroetch specimens were prepared by cutting the connections normal to the longitudinal axis of the weld at numerous locations around the branch perimeter. The macroetch specimens were scanned and the horizontal/vertical leg sizes and effective weld throats were measured using software with built-in measuring tools. Average values of the effective weld throats for individual weld elements around the branch perimeter for each test specimen were used to calculate the LRFD and nominal flexural strengths of the welded joints using the equation for the effective elastic section modulus for in-plane bending (Equation 5). Because the design requirements of AISC 360 (2010) are based solely on the limit state of shear rupture along the plane of the effective weld throat, the measured values for the vertical and horizontal weld leg sizes are not presented in this paper.

Fillet weld effective throat measurements from the macroetch specimens were taken as the distance from the weld root to the outer surface at a 45° incline to the horizontal chord surface for uncracked and cracked sections, represented by red lines shown in Figure 4. The lengths of the red lines were averaged for the individual weld elements (identified as north, south, east and west) for each test specimen. An observation from the macroetch examinations of stepped connections was that the failure plane through the fillet welds of the stepped connections was consistently at an angle between 0° and 45° to the branch fusion face.

PJP flare-bevel-groove weld effective throats were measured from the macroetch specimens as the thickness of the thinner part joined (t, t_b) less the greatest perpendicular dimension from the base metal surface to the weld surface, d, as shown in Figure 5. This method is consistent with Section J2.1 of AISC 360 (2010) and AWS D1.1 (2010) for measuring complete joint penetration groove welds in T-connections without backing and welded from one side only. Because these PJP groove welds meet the qualification requirements of Clause 4.13 of AWS D1.1 (2010) for complete joint penetration butt joints in tubular connections, they may be measured as such.

The average effective weld throat thicknesses measured from the macroetch specimens for the individual weld elements of each test specimen are summarized in Table 4. A few of these are less than the minimum values in Tables J2.3 and J2.4 of AISC 360 (2010), after grinding, to ensure that weld fracture was the critical failure mode. Because all welds were sound and carefully controlled, the minimum weld size requirement would not affect the results. Those values were used—in combination with the geometric and material properties of the HSS, as well as the material properties of the as-laid weld metal—to calculate the predicted flexural capacities of the welded joints, which are used in the analyses performed in the following sections.

Three all-weld-metal TCs were created in accordance with Clause 4 of AWS D1.1 (2010). The TCs were extracted from welded test plates that were fabricated using the same electrode spool, equipment and fabrication processes (using the average welding process parameters) as those used to fabricate the welded joints tested in the experimental program. The welding process parameters for the TCs were 24-V arc voltage, 400-ipm (inches per minute) wire feed

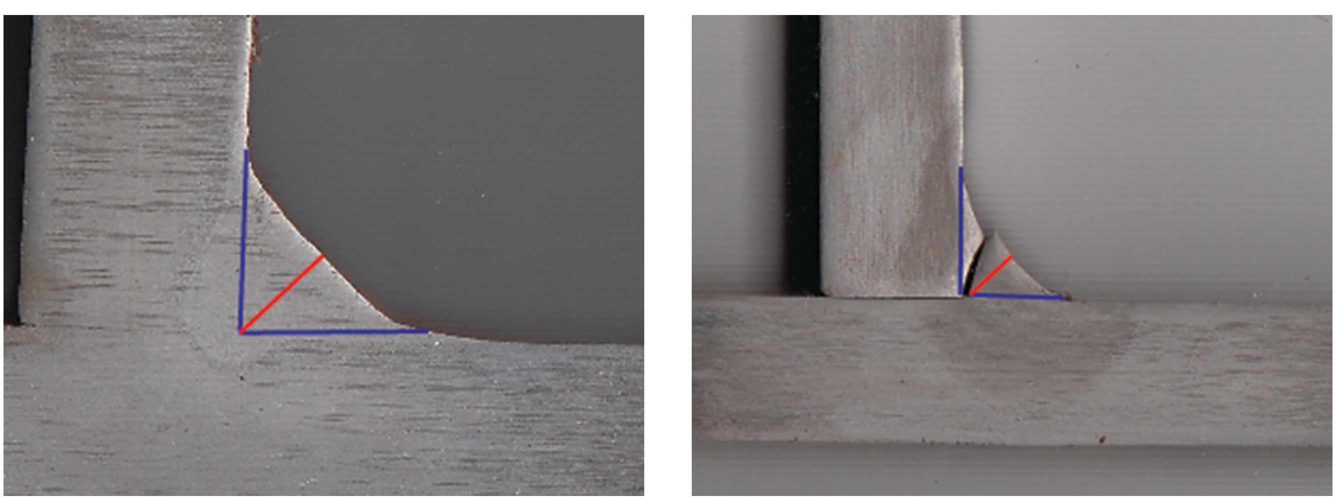

(a) (b)

Fig. 4. Example of fillet weld effective throat measurements from macroetch specimens: (a) fillet weld cross-section not cracked; (b) fully cracked fillet weld cross-section.

speed, 15-ipm travel speed and a 90% argon/10% carbon dioxide shielding gas mixture supplied at a flow rate of 40 CFH. Every TC was tested in accordance with the standard methods for tension testing of metallic materials (ASTM, 2008), and the specified yield strength of the material was determined using the 0.2% offset method. The results from three all-weld-metal TC specimens are summarized in Table 5.

All of the measured material properties exceeded the minimum requirements for AWS ER70S-6 solid-wire electrodes. The average tensile strength of the as-laid weld metal was 26% larger than the nominal specified tensile strength of 70 ksi. This contributed to undesirable failure modes observed in two of the test specimens, whereby connection failure preceded weld failure.

Results from Full-Scale Tests on Square HSS-to-HSS Moment T-Connections

Twelve full-scale square HSS-to-HSS moment T-connections subject to branch in-plane bending were tested to failure in a quasi-static manner. Figure 6 summarizes the failure modes observed during the experimental program. Ten out of 12 test specimens failed by weld rupture. Two specimens (T-0.50-34 and T-0.50-17) failed by rupture of the chord face (or punching shear) on the tension side of the connection after extensive chord face plastification. These were tested early in the experimental program and indicated that the actual tensile strength of the weld metal was likely higher than the specified nominal strength (which was later confirmed).

A summary of the actual flexural strength (or ultimate moment) of the welded joints with the predicted nominal flexural strengths of the connections, calculated using the actual geometric and material properties of the HSS material and as-laid weld metal, is provided in Table 6. Every weld-critical test specimen failed at a moment considerably higher than the predicted nominal flexural strength of the connection. Table 6 also includes the measured initial elastic rotational stiffness of each connection and the corresponding connection rotation at failure. The moment versus connection rotation relationship was determined using the magnitude of force applied by the MTS actuator and coordinates from the LED targets measured throughout testing. Initial elastic rotational stiffness was determined from the slope of the linear-elastic region of the moment versus connection rotation relationships for each test specimen.

Figures 7 through 10 show the typical distribution of normal strain observed around the branch perimeter at three load levels: the actual, nominal and LRFD flexural strengths of the welded joint. The plots demonstrate that for a wide variety of connection geometric configurations, the distribution of normal strain around the branch perimeter adjacent to the welded joint in HSS-to-HSS moment T-connections is highly nonuniform.

At the nominal and LRFD strengths, strain distribution is nearly symmetric about the theoretical neutral axis, located at strain gage (SG)-5E for specimens with $\beta = 0.25$ and SG-7E for specimens with $0.25 > \beta \leq 1.00$, which is expected for connections subject to pure in-plane bending. The strains are largest at the branch corner which is typical of semi-rigid connections because of the flexible chord face and stiff branch corners, which attract more load. As expected, the magnitude of strain along the transverse faces (relative to the magnitude of strain at the corners) decreases as β increases; hence, the effectiveness of the transverse

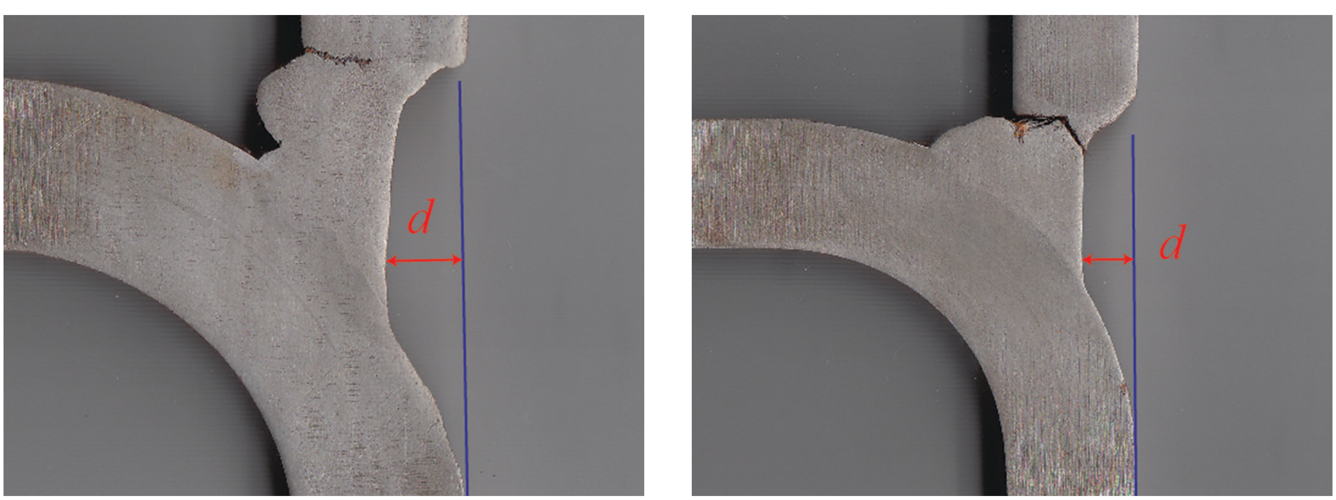

(a) (b)

Fig. 5. Example of PJP groove weld effective throat measurements from macroetch specimens: (a) PJP groove weld cross-section not fully cracked; (b) fully cracked PJP groove weld cross-section.

Table 4. Average Effective Weld Throat Thickness Measured from Macroetch Specimens				
Specimen Designation	North Weld, Transverse (in.)	South Weld, Transverse (in.)	East Weld, Longitudinal (in.)	West Weld, Longitudinal (in.)
T-0.25-34	0.102	0.097	0.089	0.088
T-0.25-23	0.094	0.128	0.095	0.051
T-0.25-17	0.090	0.101	0.092	0.094
T-0.50-34	0.150	0.158	0.170	0.170
T-0.50-23	0.154	0.133	0.168	0.180
T-0.50-17	0.259	0.280	0.290	0.272
T-0.75-34	0.112	0.087	0.068	0.134
T-0.75-23	0.139	0.124	0.137	0.120
T-0.75-17	0.237	0.200	0.158	0.277
T-1.00-34	0.128	0.078	**0.126**	**0.117**
T-1.00-23	0.180	0.232	**0.204**	**0.208**
T-1.00-17	0.240	0.311	**0.225**	**0.252**
Note: Values in bold are PJP flare-bevel-groove welds.				

Table 5. All-Weld-Metal Tensile Coupon Material Test Results				
Coupon Designation	F_{yw} (ksi)	E ($\times 10^3$ ksi)	F_{uw} (ksi)	ε_u (%)
[i]	76.2	29.6	90.0	29.2
[ii]	75.7	31.6	86.9	28.3
[iii]	75.8	29.6	87.5	28.0
Average	75.9	30.3	88.1	28.5

Table 6. Moment and Rotation Characteristics of the Tested Connections						
Specimen Designation	β-Ratio	Chord Wall Slenderness	Predicted Nominal Flexural Strength M_{n-ip} (kip-ft)	Initial Elastic Rotational Stiffness of Connection (kip-ft/radian)	Connection Rotation at Failure ($\times 10^{-3}$ radians)	Actual Flexural Strength M_u (kip-ft)
T-0.25-34	0.25	34	1.02	33.1	368	4.11
T-0.25-23	0.25	23	1.68	81.1	167	4.37
T-0.25-17	0.25	17	2.10	194	46.3	4.82
T-0.50-34*	0.50	34	4.81	N/A**	N/A**	5.61
T-0.50-23	0.50	23	7.62	343	195	15.2
T-0.50-17*	0.50	17	20.1	918	189	29.6
T-0.75-34	0.75	34	7.79	534	77.8	14.4
T-0.75-23	0.75	23	11.6	1,544	36.4	27.1
T-0.75-17	0.75	17	22.1	3,148	40.2	52.2
T-1.00-34	1.00	34	14.8	3,145	19.6	39.7
T-1.00-23	1.00	23	29.3	5,296	21.8	64.7
T-1.00-17	1.00	17	40.5	7,477	20.5	93.6

* Connection failure preceded weld rupture. Predicted nominal flexural strengths are those for the connection instead of the welded joint.
** Not available

weld element decreases. While it is evident that the transverse weld elements are less effective in resisting the applied loads, they still contribute to the flexural strength of the welded joint beyond the distance $2t$ from the longitudinal face of the branch and, hence, should not be neglected in weld resistance calculations.

At the ultimate moment, the distribution of strain is no longer symmetric about the theoretical neutral axis, indicating that plastic stress redistribution has taken place prior to failure. The magnitude of normal strain along the transverse weld elements indicates that a large portion of the weld perimeter is effective in resisting the applied loads.

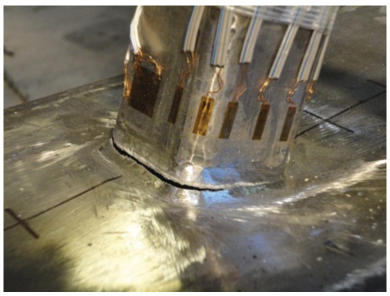

(a) T-0.25-34: weld rupture

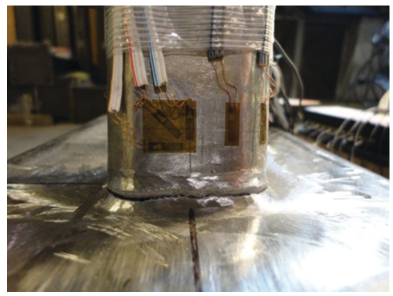

(b) T-0.25-23: weld rupture

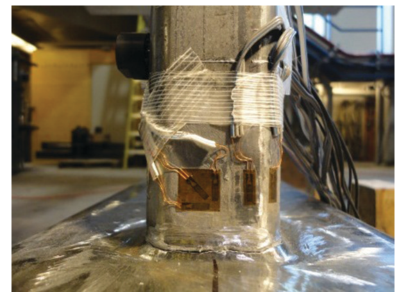

(c) T-0.25-17: weld rupture

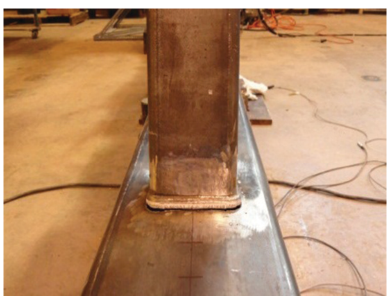

(d) T-0.50-34: chord face rupture

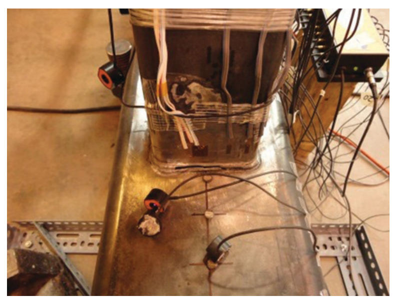

(e) T-0.50-23: weld rupture

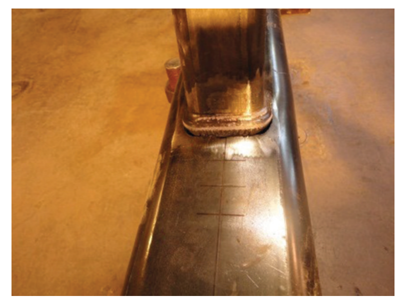

(f) T-0.50-17: chord face rupture

(g) T-0.75-34: weld rupture

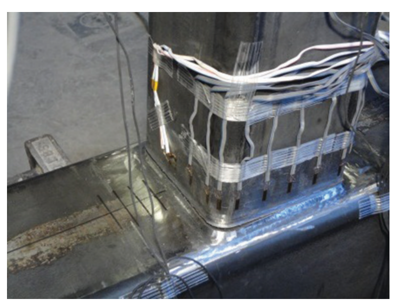

(h) T-0.75-23: weld rupture

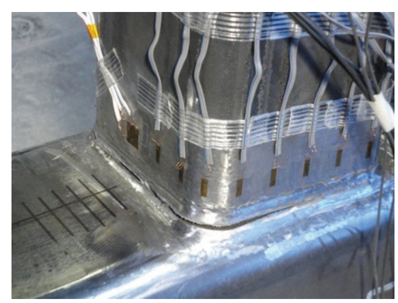

(i) T-0.75-17: weld rupture

(j) T-1.00-34: weld rupture

(k) T-1.00-23: weld rupture

(l) T-1.00-17: weld rupture

Fig. 6. Failure modes of test specimens.

EVALUATION OF RESULTS

The objective of the experimental program was to verify or adjust the current effective elastic section modulus for in-plane bending defined by Equation 5 and postulated in Table K4.1 of AISC 360 (2010) for HSS-to-HSS moment T-connections. Because test specimens T-0.50-34 and T-0.50-17 failed by chord face rupture (considered a connection failure), they are not included in the analyses performed herein. The data from the successful tests are used to plot correlations between the actual and predicted flexural strengths of the welded joints using effective weld properties for the cases excluding and including the (1.00 + 0.5 $\sin^{1.5}\theta$) fillet weld strength enhancement factor. Based on the analysis, a modification to the current effective weld properties is proposed.

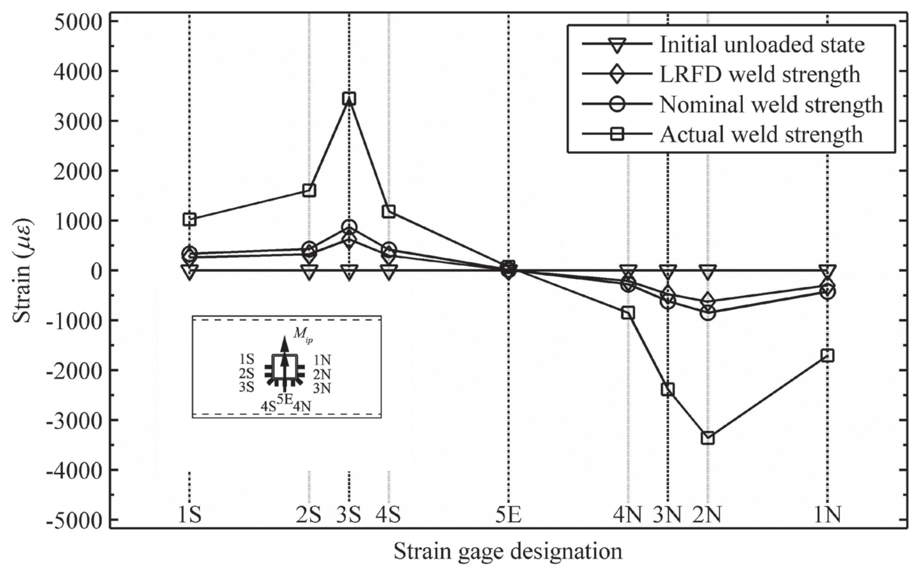

Fig. 7. Typical distribution of normal strain around the branch perimeter for specimens with $\beta = 0.25$.

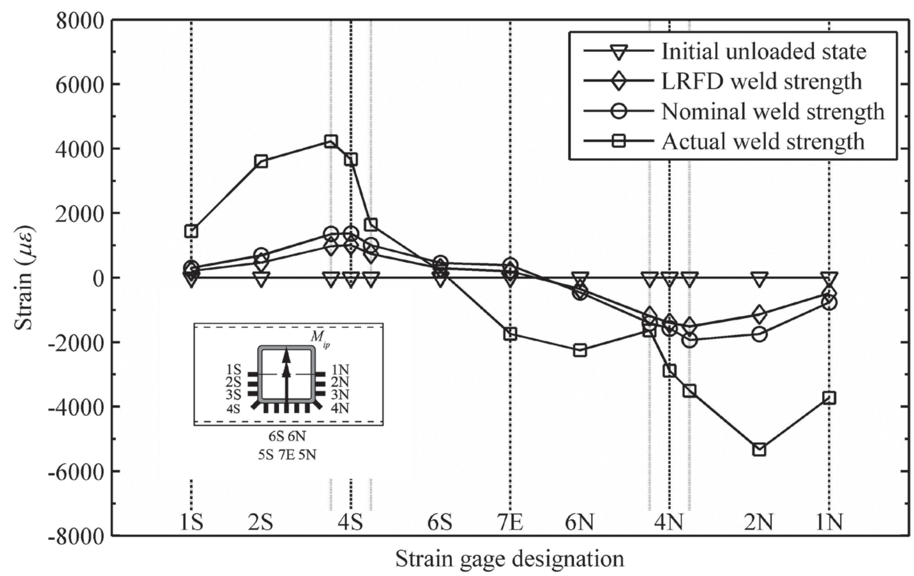

Fig. 8. Typical distribution of normal strain around the branch perimeter for specimens with $\beta = 0.50$.

Evaluation of Current Effective Weld Properties

In order to assess whether the safety margins are adequate or excessive, one can check to ensure that a minimum safety index of $\beta^+ = 4.0$ [as currently adopted by AISC 360 (2010) per Chapter B of the Specification Commentary] is achieved, using a simplified reliability analysis in which the resistance factor (ϕ) is given by Equation 12 (Fisher et al., 1978; Ravindra and Galambos, 1978):

$$\phi = m_R \exp\left(-\alpha\beta^+ \text{COV}\right) \tag{12}$$

where m_R is the mean of the ratio of actual element strength to nominal element strength, COV is the associated coefficient of variation and α is the coefficient of separation taken to be 0.55 (Ravindra & Galambos, 1978). Equation 12 neglects variations in material properties, geometric parameters and fabrication defects, relying solely on the so-called professional factor. In the absence of reliable statistical data related to welds, this is believed to be a conservative approach. Resistance factors of 0.75 and 0.80 are stipulated in Section K4 of AISC 360 (2010) to calculate the LRFD

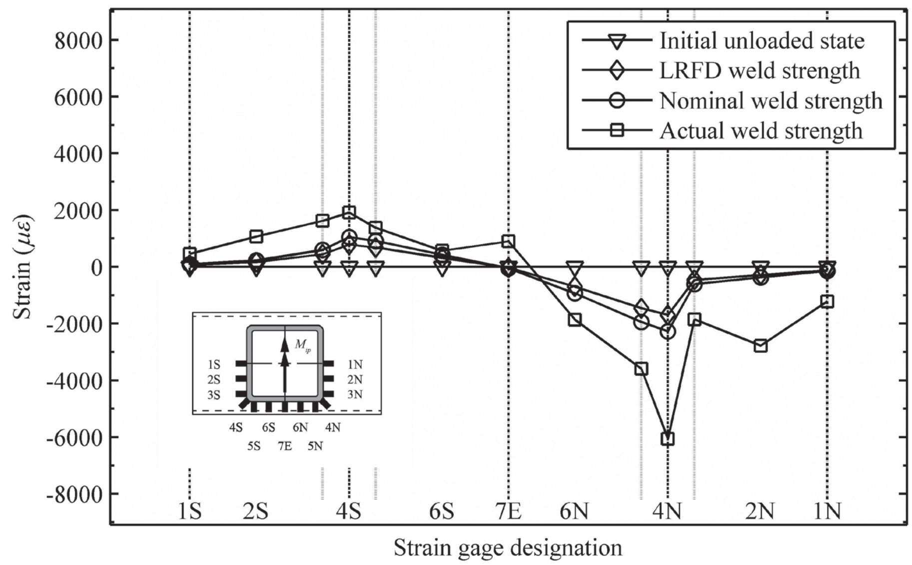

Fig. 9. Typical distribution of normal strain around the branch perimeter for specimens with $\beta = 0.75$.

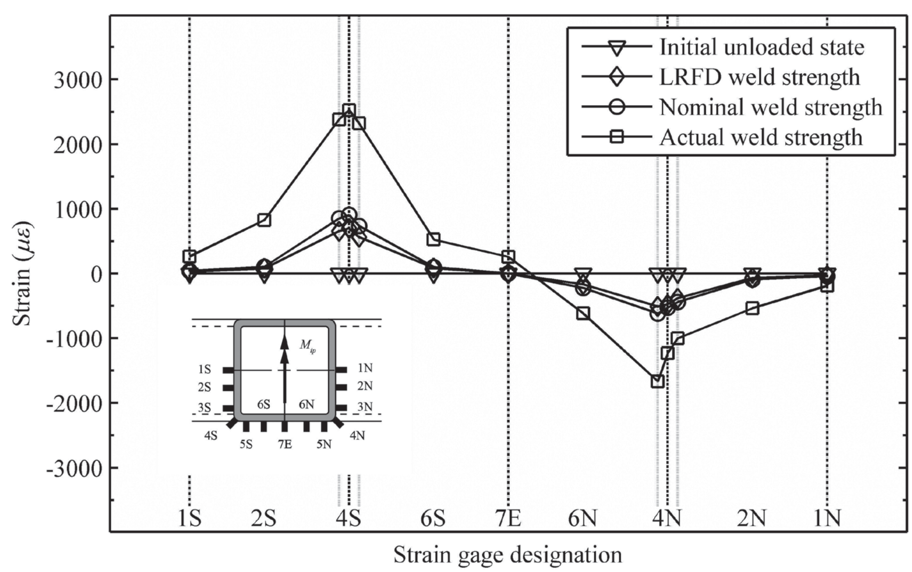

Fig. 10. Typical distribution of normal strain around the branch perimeter for specimens with $\beta = 1.00$.

Table 7. Simplified Reliability Analysis of Square HSS-to-HSS Moment T-Connections		
Experimental Designation	Actual/Nominal Excluding $(1.00 + 0.5 \sin^{1.5}\theta)$ Factor	Actual/Nominal Including $(1.00 + 0.5 \sin^{1.5}\theta)$ Factor
T-0.25-34	4.04	2.69
T-0.25-23	2.59	1.73
T-0.25-17	2.30	1.53
T-0.50-23	2.00	1.34
T-0.75-34	1.84	1.23
T-0.75-23	2.34	1.56
T-0.75-17	2.37	1.58
T-1.00-34	2.68	2.41
T-1.00-23	2.21	1.89
T-1.00-17	2.31	1.89
Mean	2.47	1.78
COV	0.245	0.258
ϕ	1.44	1.01

design strength of fillet-welded joints and PJP groove welds, respectively.

The actual flexural strengths for each weld-critical connection are summarized in Table 6 with the predicted nominal flexural strengths, which were calculated using the measured geometric and material properties of the HSS and as-laid welds. Weld sizes for the individual weld elements were taken from Table 4, which is based on average measurements of the macroetch specimens.

The mean of the actual/predicted weld strengths, as well as the COV, are given in Table 7 and used, in combination with Equation 12, to calculate a resistance factor equal to 1.44. Because this is much larger than the 0.75 and 0.80 required for fillet welds and PJP groove welds, respectively, the current equation for the effective elastic section modulus for in-plane bending can be deemed very conservative.

The predicted nominal flexural strength was recalculated with the inclusion of the $(1.00 + 0.5 \sin^{1.5}\theta)$ factor applied to fillet weld elements. For test specimens with $0.25 > \beta \leq 0.75$, all four sides are fillet-welded and loaded normal ($\theta = 90°$) to the longitudinal axis of the weld; hence, the nominal flexural strength was increased by a factor of 1.5. For the matched connections, the factor was applied only to the transverse weld elements. A resistance factor equal to 1.01 was thus calculated (see Table 7). The correlations excluding and including the $(1.00 + 0.5 \sin^{1.5}\theta)$ factor are plotted in Figures 11 and 12, respectively.

Because ϕ is still larger than the resistance factors for fillet welds and PJP groove welds, the $(1.00 + 0.5 \sin^{1.5}\theta)$ factor can be applied safely with the current equation for the effective elastic section modulus for in-plane bending for HSS-to-HSS moment T-connections. Although it may be safe for such connections, it was proven to be unsafe when applied to axially loaded T- and cross- (or X-) connections between HSS (McFadden et al., 2013). Thus, for consistency, it would not be practical to apply the $(1.00 + 0.5 \sin^{1.5}\theta)$ factor to some types of HSS connections under specific loads and not to others.

If the requirements of the Canadian Standards Association (CSA) S16 (2009) are evaluated, an identical result to AISC 360 (2010) is obtained. Although they have different resistance factors for fillet welds [equal to 0.67 and 0.75 for CSA S16 (2009) and AISC 360 (2010), respectively], the equations come out identical as shown.

For CSA S16 (2009):

$$\begin{aligned} \phi M_{n-ip} &= 0.67\phi_w \left(F_{EXX} S_{ip}\right) \\ \phi M_{n-ip} &= 0.67(0.67)\left(F_{EXX} S_{ip}\right) \\ \phi M_{n-ip} &= 0.45\left(F_{EXX} S_{ip}\right) \end{aligned} \tag{13}$$

For AISC 360 (2010):

$$\begin{aligned} \phi M_{n-ip} &= \phi\left(F_{nw} S_{ip}\right) \\ \phi M_{n-ip} &= 0.75\left(0.60 \times F_{EXX} S_{ip}\right) \\ \phi M_{n-ip} &= 0.45\left(F_{EXX} S_{ip}\right) \end{aligned} \tag{14}$$

Because ϕ is much larger than 0.67, the equation for the effective elastic section modulus for in-plane bending may be deemed very conservative for CSA S16 (2009) too.

Evaluation of Modified Effective Weld Properties

The branch strain distribution plots show that the transverse weld elements are effective in resisting the applied loads beyond the limit of two times the chord wall thickness ($2t$), and a more reasonable limit appears to be $B_b/4$. Thus, the requirement in Section K4 of AISC 360 (2010):

When $\beta > 0.85$ or $\theta > 50°$, $b_{eoi}/2$ shall not exceed $2t$

could be modified to:

When $\beta > 0.85$ or $\theta > 50°$, $b_{eoi}/2$ shall not exceed $B_b/4$

This modification to the requirement limiting the value of b_{eoi} increases the effective length of the transverse weld

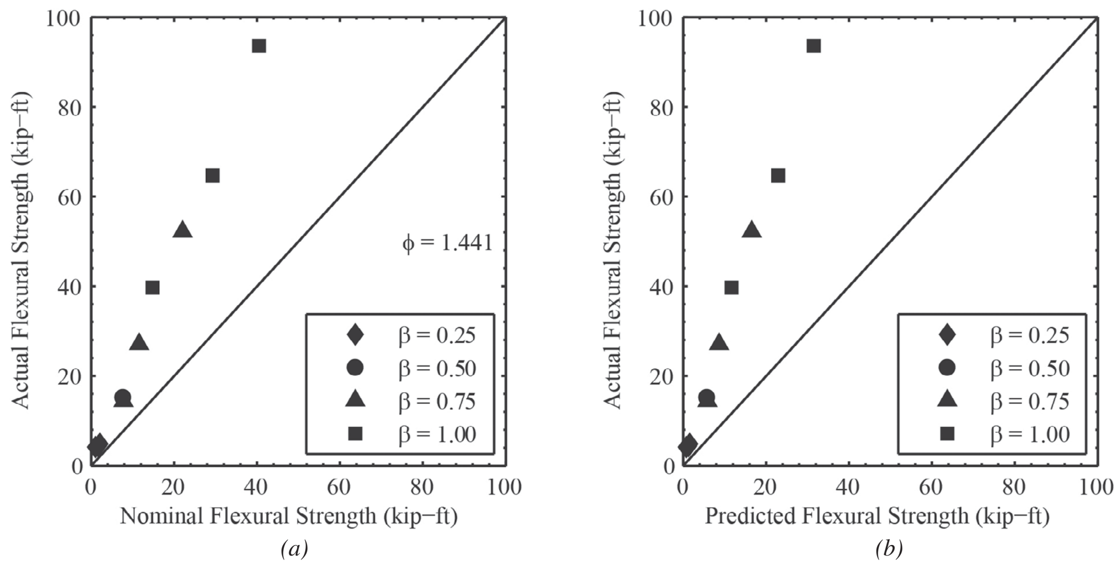

Fig. 11. Correlation with test results for square HSS-to-HSS moment T-connections and excluding the $(1.00 + 0.50 \sin^{1.5}\theta)$ term: (a) actual strength vs. predicted nominal strength ($M_{n\text{-}ip}$); (b) actual strength vs. predicted LRFD strength ($\phi M_{n\text{-}ip}$).

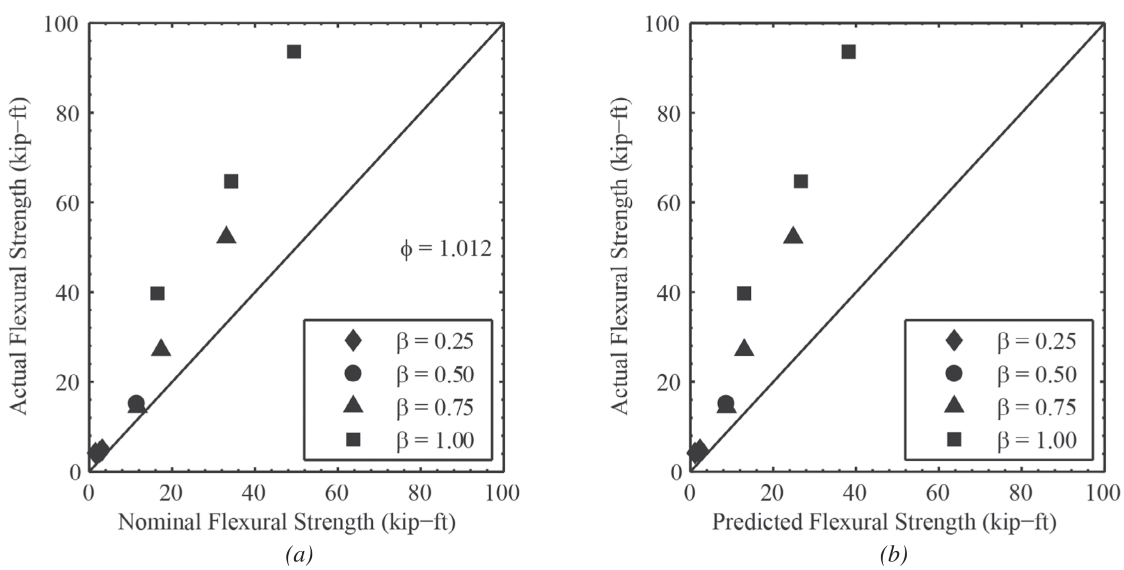

Fig. 12. Correlation with test results for square HSS-to-HSS moment T-connections and including the $(1.00 + 0.50 \sin^{1.5}\theta)$ term: (a) actual strength vs. predicted nominal strength ($M_{n\text{-}ip}$); (b) actual strength vs. predicted LRFD strength ($\phi M_{n\text{-}ip}$).

Table 8. Actual versus Predicted Nominal Flexural Strength Using the b_{eoi} Modification and Excluding the $(1.00 + 0.5 \sin^{1.5}\theta)$ Factor			
Experimental Designation	Actual Flexural Strength M_u (kip-ft)	Predicted Nominal Flexural Strength M_{n-ip} (kip-ft)	Actual/Nominal
T-0.25-34	4.11	1.02	4.04
T-0.25-23	4.37	1.43	3.06
T-0.25-17	4.82	1.41	3.43
T-0.50-23	15.2	9.22	1.65
T-0.75-34	14.4	10.8	1.34
T-0.75-23	27.1	17.0	1.60
T-0.75-17	52.2	28.9	1.81
T-1.00-34	39.7	19.9	2.00
T-1.00-23	64.7	44.2	1.46
T-1.00-17	93.6	62.0	1.51
		Mean	2.19
		COV	0.437
		ϕ	0.836

elements, which ultimately leads to an increased predicted flexural strength. An exception is for small HSS branch member sizes, such as for HSS 2×2×¼, where this modified requirement actually decreases the effective length of the transverse welds. This results in an even more conservative approach (which was shown in the previous section to already be very conservative).

The correlations in Table 7 and Figure 11 have been recalculated with the b_{eoi} modification, excluding the $(1.00 + 0.5 \sin^{1.5}\theta)$ factor, and the results are summarized in Table 8 and plotted in Figure 13. As shown, the modification provides a resistance factor equal to 0.836, which is larger than those for fillet welds and PJP groove welds; hence, the modified requirement can be deemed adequately conservative for such connections for AISC 360 (2010) and CSA S16 (2009).

The proposed b_{eoi} modification is also potentially applicable to the equations for the effective length under branch axial load (Equation 4) and the effective elastic section modulus for out-of-plane bending (Equation 6). While there are no available test data on weld-critical connections between square/rectangular HSS loaded by branch out-of-plane bending, the data from weld-critical axially loaded T- and X- (or cross-) connection tests performed at the University of Toronto (Packer and Cassidy, 1995) can be reanalyzed using the modified requirement to investigate whether it remains a conservative assumption. Performing a simplified reliability analysis on the data gives a mean value of the actual/predicted strengths equal to 1.11 and a COV equal to 0.141 for a calculated resistance factor, ϕ, equal to 0.820. Because this is larger than 0.75, which is required for fillet welds, the modified requirements to the effective weld properties in Table K4.1 (AISC, 2010) proposed in this section may also be deemed adequately conservative for axially loaded HSS-to-HSS T- and X- (or cross-) connections. Figure 14 shows the correlation with the test results from that study (Packer and Cassidy, 1995).

The correlations including the fillet weld directional strength enhancement factor are plotted in Figures 15 and 16 for 90° square HSS-to-HSS moment T-connections (this study) and axially loaded HSS-to-HSS T- and X- (or cross-) connections (Packer and Cassidy, 1995), respectively. Because each produces a resistance factor, ϕ, considerably less than 0.75, the fillet weld directional strength enhancement factor equal to $(1.00 + 0.5 \sin^{1.5}\theta)$ should not be used for such connections in combination with the modified requirement proposed herein to the Table K4.1 (AISC, 2010) effective weld properties.

CONCLUSIONS AND RECOMMENDATIONS

Based on the results from this experimental program, which consisted of 12 full-scale tests on square HSS-to-HSS moment T-connections designed to be weld-critical, and on the reanalysis of data from previous experimental programs consisting of full-scale tests on weld-critical connections between HSS (Packer and Cassidy, 1995), the following conclusions and recommendations are made:

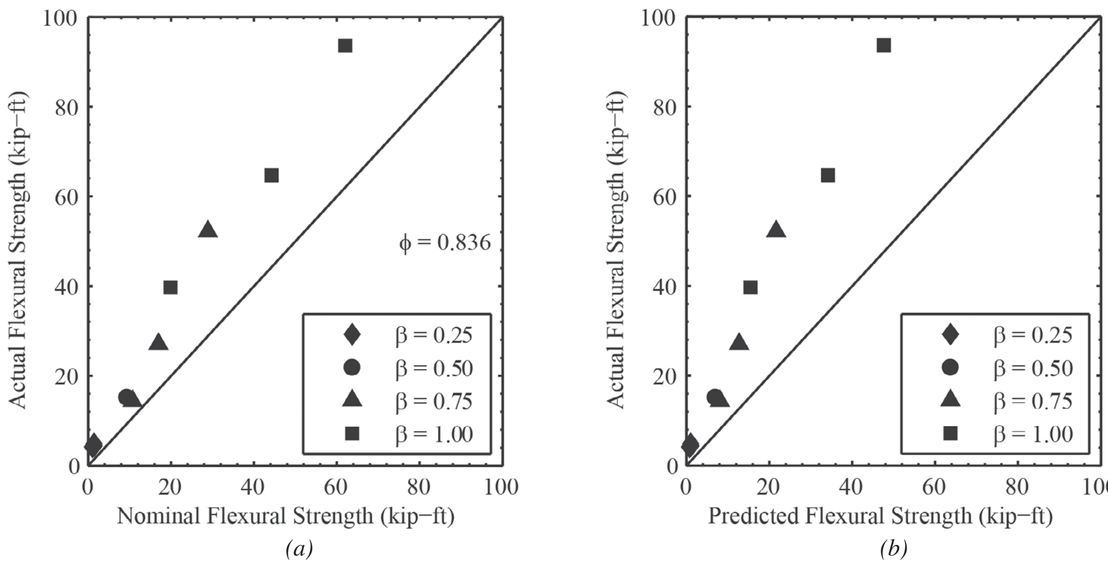

Fig. 13. Correlation with test results for square HSS-to-HSS moment T-connections using the modification to AISC 360 (2010) and excluding the $(1.00 + 0.5\ \sin^{1.5}\theta)$ factor: (a) actual strength vs. predicted nominal strength (M_{n-ip}); (b) actual strength vs. predicted LRFD strength (ϕM_{n-ip}).

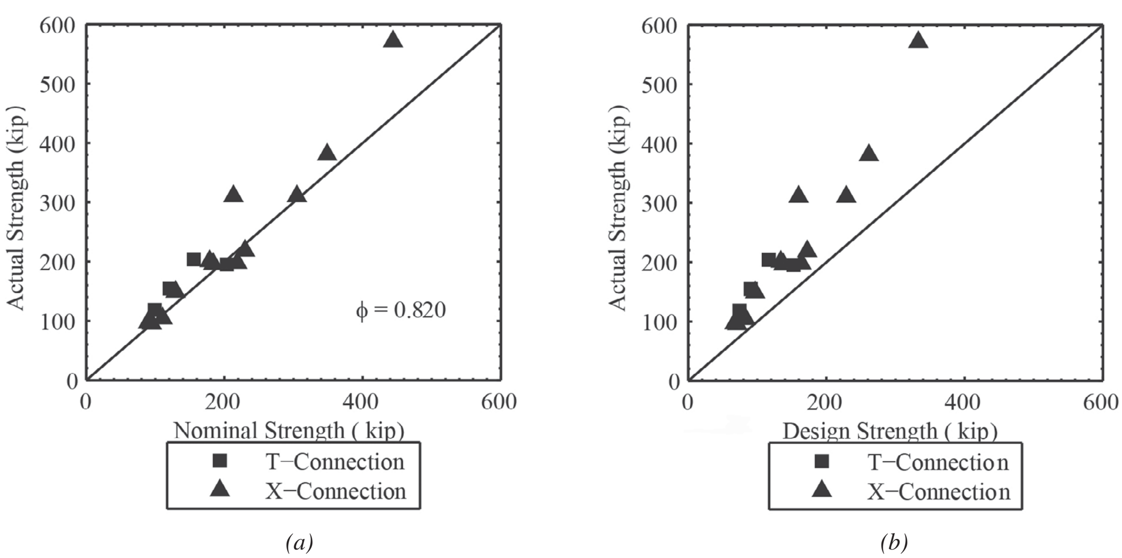

Fig. 14. Correlation with test results for HSS-to-HSS axially-loaded T- and X-connections (Packer and Cassidy, 1995) using the modification to AISC 360 (2010) and excluding the $(1.00 + 0.5\ \sin^{1.5}\theta)$ factor: (a) actual strength vs. predicted nominal strength (R_n); (b) actual strength vs. predicted LRFD strength (ϕR_n).

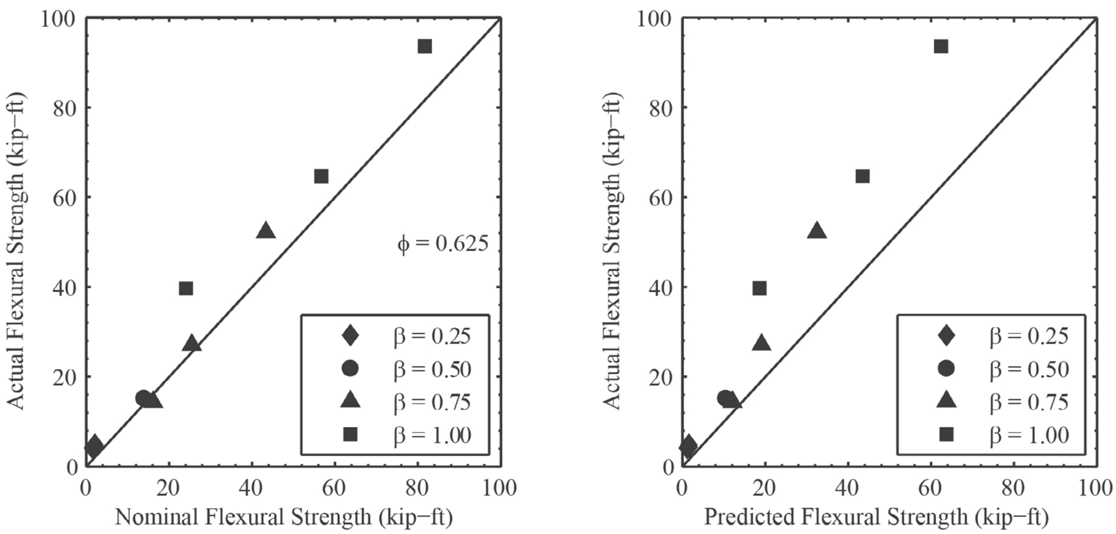

(a) (b)

Fig. 15. Correlation with test results for square HSS-to-HSS moment T-connections using the modification to AISC 360 (2010) and including the $(1.00 + 0.5 \sin^{1.5}\theta)$ factor: (a) actual strength vs. predicted nominal strength (M_{n-ip}); (b) actual strength vs. predicted LRFD strength (ϕM_{n-ip}).

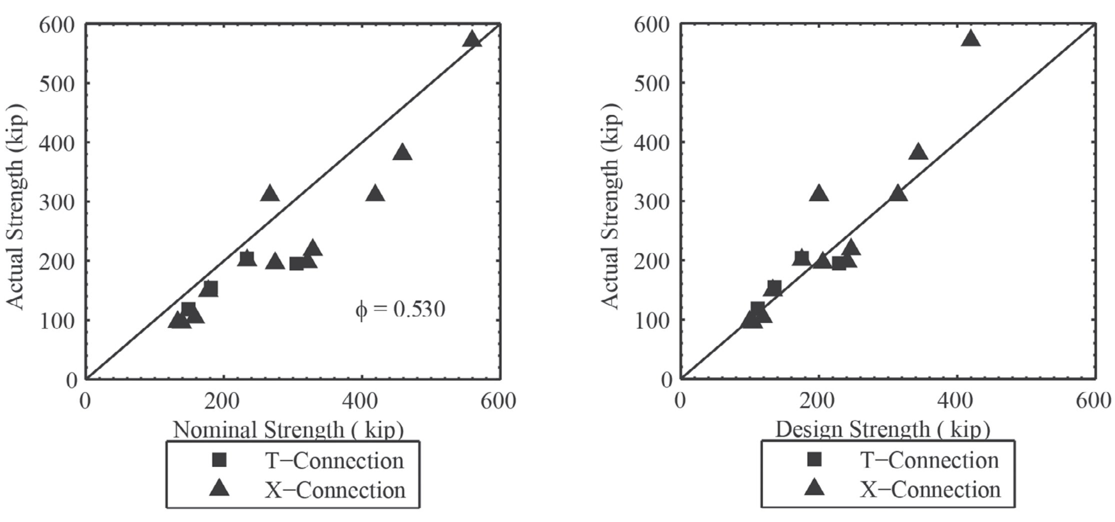

(a) (b)

Fig. 16. Correlation with test results for HSS-to-HSS axially-loaded T- and X-connections (Packer and Cassidy, 1995) using the modification to the AISC 360 (2010) and including the $(1.00 + 0.5 \sin^{1.5}\theta)$ factor: (a) actual strength vs. predicted nominal strength (R_n); (b) actual strength vs. predicted LRFD strength (ϕR_n).

- The $(1.00 + 0.50 \sin^{1.5}\theta)$ factor (or fillet weld directional strength enhancement factor) should not be universally applied to all connections between HSS, when the effective length method is used, because it may result in an unsafe design. This may be because connections with HSS are inherently eccentrically loaded (because welding can only be performed on one side of the branch wall) and secondary effects create additional tension at the fillet weld roots.
- Macroetch specimens of the failed welds showed that the angle of the failure plane through the weld, for stepped connections that are fillet-welded all-around the branch perimeter, is between 0 and 45° to the branch fusion face.
- The distribution of normal strain around the branch perimeter adjacent to the welded joint in a HSS-to-HSS T-connection subject to branch in-plane bending is highly nonuniform.
- As the β-ratio for HSS-to-HSS moment T-connections decreases, the effective length of the weld element along the transverse walls of the branch increases (and vice versa).
- The current equation for the effective elastic section modulus for in-plane bending specified in Table K4.1 of AISC 360 (2010) is very conservative and can be considered a lower bound, safe design approach.
- Modifying the requirement that limits the effective width, b_{eoi}, in Table K4.1 (AISC, 2010) from:

  When $\beta > 0.85$ or $\theta > 50^\circ$, $b_{eoi}/2$ shall not exceed $2t$

  to:

  When $\beta > 0.85$ or $\theta > 50^\circ$, $b_{eoi}/2$ shall not exceed $B_b/4$

  increases the predicted strength of welded joints in square HSS-to-HSS moment T-connections subject to branch bending. Adopting this modification is still conservative (Figure 13) and generally provides a more economical design approach, within the parameter range of $t_b \leq t$ studied. Furthermore, if the same modification ($b_{eoi}/2 \leq B_b/4$) is extended to previous weld-critical tests on HSS-to-HSS T- and X- (or cross-) connections (Packer and Cassidy, 1995), subject to branch axial loading, then reanalysis of those test results shows that the proposed effective length modification is also acceptable for those connections (Figure 14).

ACKNOWLEDGMENTS

The authors are grateful for the financial support of the American Institute of Steel Construction and the advice of the AISC project steering committee, to Lincoln Electric for fabrication of test specimens, to Atlas Tube for donation of the HSS members, to the laboratory staff at the University of Toronto Structural Testing Facility and to Mr. V. Kan and Mr. T. Pereira (summer research students) for laboratory assistance.

SYMBOLS

A	Cross-sectional area of HSS, in.^{2}
B	Overall width of HSS chord, measured normal to the plane of the connection, in.
B_b	Overall width of HSS branch, measured normal to the plane of the connection, in.
COV	Coefficient of variation
E	Young's modulus, ksi
F_{EXX}	Filler metal classification strength, ksi
F_{nw}	Nominal stress of weld metal, ksi
F_u	Ultimate tensile strength of HSS, ksi
F_{uw}	Ultimate tensile strength of weld metal, ksi
F_y	Yield stress of HSS, ksi
F_{yb}	Yield stress of HSS branch, ksi
F_{yw}	Yield stress of weld metal, ksi
GMAW	Gas-metal arc welding
H	Overall height of HSS chord, measured in the plane of the connection, in.
H_b	Overall height of HSS branch member, measured in the plane of the connection, in.
I_{ip}	Moment of inertia for in-plane bending, in.^{4}
I_{op}	Moment of inertia for out-of-plane bending, in.^{4}
M_{ip}	Applied in-plane bending moment, kip-in.
M_{op}	Applied out-of-plane bending moment, kip-in.
$M_{n\text{-}ip}$	Nominal flexural strength of weld for in-plane bending (AISC, 2010), kip-in. or kip-ft.
$M_{n\text{-}op}$	Nominal flexural strength of weld for out-of-plane bending (AISC, 2010), kip-in. or kip-ft.
M_u	Ultimate flexural strength for in-plane bending, kip-in. or kip-ft.

P Applied force, kip

P_n Nominal axial strength, kip

R_n Nominal strength of HSS member, ksi

SG Strain gage

S_{ip} Effective elastic section modulus of weld for in-plane bending (AISC, 2010), in.^{3}

S_{op} Effective elastic section modulus of weld for out-of-plane bending (AISC, 2010), in.^{3}

b_{eoi} Effective width of the branch face welded to the chord, in.

d Greatest perpendicular dimension measured from a line flush to the base metal surface to the weld surface, in.

l_e Effective weld length of groove and fillet welds for HSS, in.

m_R Mean of the ratio (actual element strength/nominal element strength)

t Wall thickness of HSS chord member, in.

t_b Wall thickness of HSS branch member, in.

t_w Effective weld throat around the perimeter of the branch, in.

α Coefficient of separation (taken equal to 0.55)

β Width ratio; the ratio of overall branch width to chord width for HSS

β^+ Safety index (taken equal to 4.00)

ε_u Elongation at rupture, ultimate strain, in./in.

ε_y Strain at material yield point, in./in.

ϕ Resistance factor (associated with the LRFD design method)

ϕ_w Resistance factor for welded joints according to CSA (2009) equal to 0.67

θ Included angle between the branch and chord, degrees; angle of loading measured from the weld longitudinal axis, degrees

REFERENCES

AISC (2010), ANSI/AISC 360-10, *Specification for Structural Steel Buildings*, American Institute of Steel Construction, Chicago, IL.

ASTM (2008), E8/E8M-08, *Standard Test Methods for Tension Testing of Metallic Materials*, American Society for Testing Materials, West Conshohocken, PA.

ASTM (2010), ASTM A500/A500M-10, *Standard Specification for Cold-Formed Welded and Seamless Carbon Steel Structural Tubing in Rounds and Shapes*, American Society for Testing Materials, West Conshohocken, PA.

AWS (2010), ANSI/AWS D1.1/D1.1M:2010, *Structural Welding Code—Steel, 22*, American Welding Society, Miami, FL.

CSA (2009), CSA S16-09. *Design of Steel Structures*, Canadian Standards Association, Toronto, ON, Canada.

Davies, G. and Packer, J.A. (1982), "Predicting the Strength of Branch Plate—RHS Connections for Punching Shear," *Canadian Journal of Civil Engineering,* Vol. 9, No. 3, pp. 458–467.

Fisher, J.W., Galambos, T. V., Kulak, G.L. and Ravindra, M.K. (1978), "Load and Resistance Factor Design Criteria for Connectors," *Journal of the Structural Division,* ASCE, Vol. 104, No. 9, pp. 1427–1441.

Frater, G.S. and Packer, J.A. (1992a), "Weldment Design for RHS Truss Connections, I: Applications," *Journal of Structural Engineering*, ASCE, Vol. 118, No. 10, pp. 2784–2803.

Frater, G.S. and Packer, J.A. (1992b), "Weldment Design for RHS Truss Connections, II: Experimentation," *Journal of Structural Engineering*, ASCE, Vol. 118, No. 10, pp. 2804–2820.

IIW (1989), Doc. XV-701-89, *Design Recommendations for Hollow Section Joints—Predominantly Statically Loaded,* 2nd ed., International Institute of Welding, Paris, France.

IIW (2012), Doc. XV-1402-12, *Static Design Procedure for Welded Hollow Section Joints—Predominantly Statically Loaded,* 3rd ed., International Institute of Welding, Paris, France.

ISO (2013), ISO 14346:2013(E), *Static Design Procedure for Welded Hollow-Section Joints—Recommendations*, International Standards Organization, Geneva, Switzerland.

McFadden, M.R., Sun, M. and Packer, J.A. (2013), "Weld Design and Fabrication for RHS Connections," *Steel Construction,* Vol. 6, No. 1, pp. 5–10.

Mehrotra, B.L. and Govil, A.K. (1972), "Shear Lag Analaysis of Rectangular Full-Width Tube Connections," *Journal of the Structural Division,* ASCE, Vol. 98, No. ST1, pp. 287–305.

Packer, J.A. and Cassidy, C.E. (1995), "Effective Weld Length for HSS T, Y, and X Connections," *Journal of Structural Engineering,* ASCE, Vol. 121, No. 10, pp. 1402–1408.

Packer, J.A., Sherman, D.R. and Lecce, M. (2010), *Steel Design Guide 24: Hollow Structural Section Connections,* American Institute of Steel Construction, Chicago, IL.

Ravindra, M.K. and Galambos, T.V. (1978), "Load and Resistance Factor Design for Steel," *Journal of the Structural Division,* ASCE, Vo. 104, No. 9, pp. 1337–1353.